Efficient photoconductive terahertz detector with all-dielectric optical metasurface

Oleg Mitrofanov, Thomas Siday, Robert J. Thompson, Ting Shan Luk, Igal Brener, and John L. Reno

Citation: APL Photonics **3**, 051703 (2018); doi: 10.1063/1.5011420
View online: https://doi.org/10.1063/1.5011420
View Table of Contents: http://aip.scitation.org/toc/app/3/5
Published by the American Institute of Physics

APL PHOTONICS **3**, 051703 (2018)

Efficient photoconductive terahertz detector with all-dielectric optical metasurface

Oleg Mitrofanov,[1,2,a] Thomas Siday,[1] Robert J. Thompson,[1] Ting Shan Luk,[2,3] Igal Brener,[2,3] and John L. Reno[2,3]
[1]*University College London, Electronic and Electrical Engineering, London WC1E 7JE, United Kingdom*
[2]*Center for Integrated Nanotechnologies, Sandia National Laboratories, Albuquerque, New Mexico 87123, USA*
[3]*Sandia National Laboratory, Albuquerque, New Mexico 87185, USA*

(Received 31 October 2017; accepted 15 January 2018; published online 9 February 2018)

We designed an optically thin photoconductive channel as an all-dielectric metasurface comprising an array of low-temperature grown GaAs nanobeams and a sub-surface distributed Bragg reflector. The metasurface exhibited enhanced optical absorption, and it was integrated into a photoconductive THz detector, which showed high efficiency and sensitivity as a result. The detector produced photocurrents over one order of magnitude higher compared to a similar detector with an unstructured surface with only 0.5 mW of optical excitation while exhibiting high dark resistance required for low-noise detection in THz time-domain spectroscopy and imaging. At that level of optical excitation, the metasurface detector showed a high signal to noise ratio of 10^6. The detector showed saturation above that level.
https://doi.org/10.1063/1.5011420

Detection of terahertz (THz) radiation with high sensitivity and efficiency remains a challenging problem for THz technology development.[1] Among the most sensitive and widely used room-temperature coherent THz detectors are ultrafast photoconductive switches.[2–4] One of the factors limiting the detector efficiency and bandwidth is the size of the photoconductive channel. For efficient photo-carrier generation, the channel thickness is typically made comparable to the optical absorption length, which is in the range of 1 μm for bulk direct bandgap semiconductors.[5] The absorption length however exceeds the photo-carrier drift length leading to recombination of the majority of photo-carriers before reaching the metallic contacts.

A THz photoconductive detector with a nanoscale channel was demonstrated recently using a single GaAs nanowire.[6] However achieving sub-picosecond photo-carrier lifetime and enabling efficient photo-excitation of semiconductor nanowires remain challenging. Plasmonic nano-antennas and gratings, and ultrathin optical cavities enabled nanoscale engineering of the active region in THz optoelectronic devices.[7–13] It allowed obtaining higher photocurrents and smaller capacitance, which lead to improvements in the response speed and efficiency of the detectors. The nanoscale active regions also enabled more sensitive THz near-field probes.[11,12] Plasmonic nanostructures however introduce Ohmic losses, which can substantially reduce the responsivity of THz detectors. For example, the Ohmic losses were estimated to be as high as 40% for a detector with a 50 nm thick photoconductive layer, reducing the benefits gained due to the plasmonic nano-antennas.[14]

Alternatively, efficiency of photoconductive THz detectors can be enhanced by using all-dielectric metasurfaces; this approach has not yet been investigated. Nanoscale dielectric structures support optical resonances,[15] and a metasurface containing only dielectric, instead of plasmonic

[a]Author to whom correspondence should be addressed: o.mitrofanov@ucl.ac.uk.

nanostructures, can be designed to trap the incident light in a selected spectral range and thus enhance optical absorption.[16–22] The aim of this study is to exploit the concepts of all-dielectric metasurfaces in THz photoconductive devices. We propose and demonstrate a THz photoconductive detector with an optically thin nanostructured photoconductive layer, which enhances optical absorption, thus promising efficient ultrathin THz detectors. We found that the nanostructured channel improved the optoelectronic properties of the detector: it increased the photocurrent induced by the THz field by over one order of magnitude, whereas the dark resistivity of the channel was found high compared to bulk devices, ensuring a high ON/OFF ratio, and thus leading to sensitive and efficient THz detection. Required optical excitation power (average) for reaching optimum THz detection operation was only 500 μW.

The nanostructured channel consists of *nanobeams* etched in a thin layer of low-temperature (LT) grown GaAs and a distributed Bragg reflector (DBR) underneath. This metasurface is designed to support a confined mode, as our numerical modeling and experimental results confirmed. The structure efficiently absorbs ultrafast optical excitation, and owing to the sub-picosecond carrier lifetime in LT GaAs, it can be quickly switched between the conductive and resistive states. We designed and fabricated a photoconductive THz detector with the metasurface incorporated into the gap of a 100 μm long THz dipole antenna.

The nanostructured photoconductive region is schematically illustrated in Fig. 1(a). It comprises an array of nanobeams etched on the surface of a ~160 nm thick LT GaAs epilayer. The period of the array was 280 nm, and the height of nanobeams was ~70 nm. The width of the beams was varied in this study to enable wavelength tuning of the resonance. This structure absorbs ~80% within a 10 nm band, which can be matched to the spectrum of a femtosecond pulse Ti:sapphire laser.

Figure 1(b) shows a numerically obtained electric field profile at 800 nm in a plane perpendicular to the nanobeam axis. The electric field distribution has a circular pattern with the center located in the middle of the channel layer, underneath the nanobeam [Fig. 1(b)]. While the circular field distribution inside the channel is similar to a magnetic dipole resonance, the field pattern above the channel, in the low-permittivity dielectric, appears as the electric dipole-like distribution.

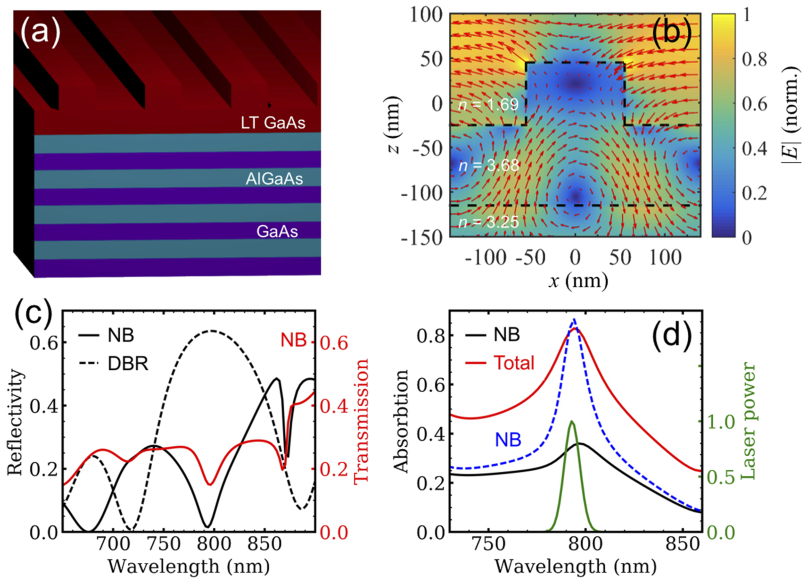

FIG. 1. (a) Schematic of the all-dielectric metasurface for enhanced optical absorption containing nanobeams and the DBR. (b) Electric field distribution in the nanobeam region at the resonance wavelength (800 nm). The arrows show the electric field vector. (c) Numerically evaluated transmission and reflection spectra. (d) Numerically evaluated absorption spectra for the structure in (a): total absorption (red), absorption in the top channel for the DBR with absorbing GaAs layers (black) and for the DBR without absorption (dashed blue). A typical spectrum of the ultrafast laser excitation is shown in green.

Furthermore, the excitation couples to the neighboring nanobeams and the distributed Bragg reflector. The nature of the resonance in this structure therefore is more complex than the classical Mie resonances.[15]

This field distribution represents a confined mode, which can be observed as dips in reflectivity and transmission spectra [Fig. 1(c)], and more clearly in the absorption spectrum [Fig. 1(d)] evaluated numerically,[23] where a 50 nm wide absorption peak rises above the typical spectrum of GaAs absorption.[4] We note that the optical properties of this mode are similar to the mode in a hybrid cavity consisting of a plasmonic nano-antenna array and DBR.[12,14]

The metasurface in Fig. 1(a) was fabricated as 20×20 μm^2 patches with the nanobeam width varied from 80 nm to 180 nm (fabrication details are summarized at the end of the letter). The variation allowed us to "tune" the mode wavelength and optimize absorption of the optical excitation. Two identical nanobeam patches of each width were fabricated: one was used for reflectivity characterization and the other was used for integration with a THz antenna to form a THz detector, as shown in Fig. 2. Another reference THz antenna with the same dimensions was fabricated 150 μm away on the flat LT GaAs layer. Both antennas were connected to the same transmission lines for direct comparison.

The THz detectors were tested in a THz time-domain spectroscopy system with a 1 mm thick ZnTe crystal used for generation of THz pulses via optical rectification of 100 fs pulses (800 nm, repetition rate: 78 MHz, average power: 400 mW). Details can be found in Ref. 14. The generated THz beam was focused (diameter: 500 μm) on the detectors. No solid immersion lens was used for further focusing to minimize sensitivity to the THz detector alignment. The detectors were photoexcited in the THz antenna gap by optical pulses from the same laser (excitation beam diameter ~2.5 μm).

Both the metasurface and the reference detectors recorded similar waveforms of the THz pulse; however, the metasurface detector exhibited ~15 times higher photocurrent (Fig. 3). The metasurface detector showed excellent frequency response [Fig. 3(b)]. Identical THz pulse waveform shapes with increasing amplitudes were detected for the optical excitation powers of 0.5 mW, 1 mW, and 2 mW (see the supplementary material). To determine optimal detector performance conditions, the peak

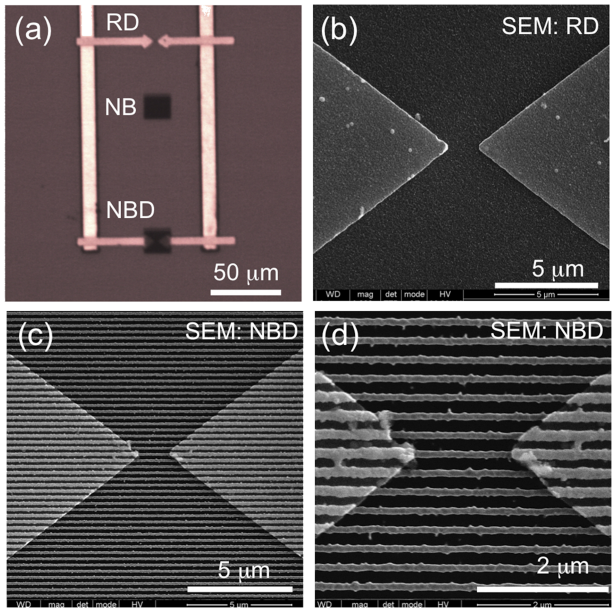

FIG. 2. The photoconducting THz detector incorporating nanobeams (NBD) and reference THz detector (RD) fabricated on the same chip. (a) Optical image showing both detectors connected to the same transmission line, and a 20×20 μm^2 patch with nanobeams (NB) used for correlation of the detector performance with the reflectivity spectrum. SEM images of the two detectors [(b) and (c)] and (d) a close-up image of the antenna gap (the active region) of NBD.

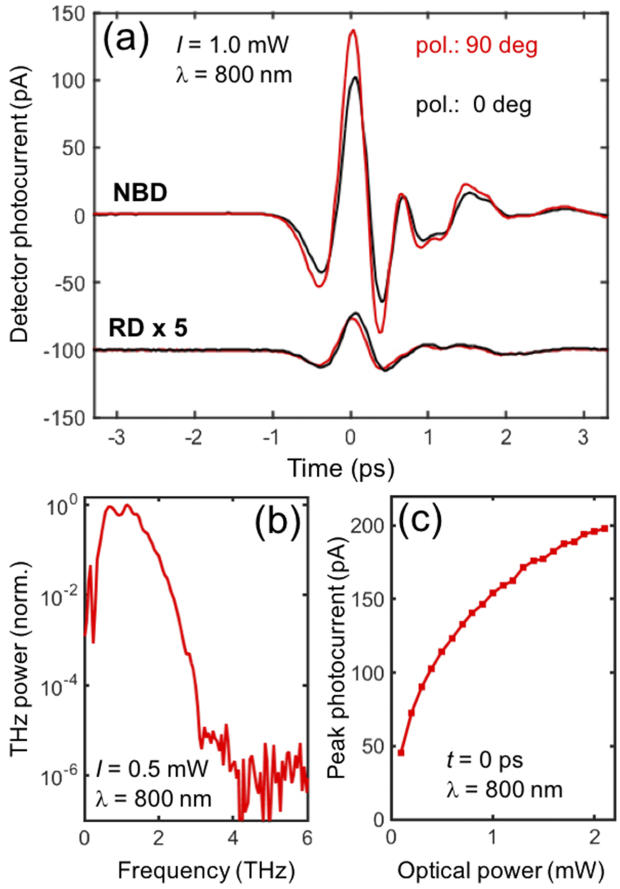

FIG. 3. THz pulse detected by the metasurface detector (NBD) and the reference detector (RD) signal: (a) time-domain trace and (b) the Fourier spectrum. (c) The NBD peak photocurrent as a function of the incident optical excitation power.

photocurrent was measured as a function of the optical excitation pulse power. It showed a saturation behavior above 0.5 mW [Fig. 3(c)]. Although the photocurrent response continued to increase with the excitation power above 0.5 mW, the noise level also increased, and there was marginal improvement in the signal-to-noise ratio of $\sim 10^6$ [Fig. 3(b)]. It indicates that the laser noise was the dominant noise source for the excitation power above 0.5 mW. We therefore conclude that the metasurface detector performed optimally with only 0.5 mW of optical excitation, which is several times lower than the power required for typical photoconductive detectors made of bulk LT GaAs.[2,4] We expect that the signal-to-noise ratio in the unpatterned detector can also reach the level of 10^6 at higher excitation powers (~5-10 mW), although we did not investigate this. We note that the dark resistance of the tested detectors was >10 GΩ, ensuring a large ON/OFF resistance ratio required for low-noise operation of photoconductive THz detectors.

To verify the origin of the response enhancement, we characterized the reflectivity of the nanostructure and compared it to the reflectivity spectrum of the reference detector surface (Fig. 4). For direct comparison, the reflectivity spectra were normalized to that of a gold patch fabricated next to the detectors on the same GaAs surface.[24] The spectrum of the unpatterned surface showed a clear DBR stop band between 750 nm and 850 nm. We note that the 160 nm layer of LT GaAs corresponds to ~3/4λ in GaAs and thus it acts as the first layer of the DBR. We estimated that about 10% of the incoming light is absorbed in the layer. In contrast, the nanobeam spectrum showed a drop in reflectivity down to ~5% at the center of the stop band for the polarization perpendicular to the nanobeams, as expected for the resonant mode (Fig. 1). Based on our numerical simulations, ~40% on the incident photons are absorbed in the photoconductive layer. We attribute the reduction in reflectivity in the center of the DBR stop band to the destructive interference of the waves reflected

by the DBR and the wave scattered by the nanobeams, similar to the effect in the cavity consisting of the DBR and the nano-antenna array.[14]

The experimental spectra (Fig. 4) and the performance of the THz detectors (Fig. 3) consistently showed a lower reflectivity at 800 nm and a higher detector response for the TM polarization, where the incident electric field vector is perpendicular to the nanobeam axis (Fig. 4), whereas a conventional detector showed almost identical properties for the two polarizations (Fig. 3). This is consistent with the simulated mode in Fig. 1(b), which is excited by the incident light with the polarization direction perpendicular to the nanobeam axis.

The enhanced optical absorption due to the nanostructured surface largely contributes to the higher photocurrent response of the metasurface THz detector compared to the reference detector; however, we found that the increase in absorption within the photoconductor was insufficient to account for the over 10 times increase of the responsivity. Another contributing factor could be a larger contact area between the antenna tips and the semiconductor in the case of the nanopatterned detector.

We note that the optical field [Fig. 1(b)] is distributed not only within the photoconductive channel but also within the DBR. Photocarriers generated in the DBR however do not contribute to the photocurrent. Our numerical estimations indicate that ~40% of the incident light is absorbed in the DBR if GaAs is used for the high-index DBR layers, as in this study. To avoid the parasitic absorption in the DBR, non-absorbing materials, such AlGaAs with Al composition above ~20% should be used for the high index layer. In that case, the photoconductive channel absorbs over 80% of the laser excitation [Fig. 1(d)].

We found that the enhanced optical absorption effect occurred for nanobeams of different widths. Structures with the width ranging from 80 to 110 nm showed a small shift in the position of the reflectivity dip (see the supplementary material) with the minima of reflectivity below 5%. The deviation of the minimum reflectivity wavelength from the target (800 nm) due to the variation of nanobeam width can be compensated by tuning the excitation laser wavelength to the wavelength of the reflectivity minimum.

The proposed THz detector can be improved further: the antenna gap can be reduced from 1.5 μm to 200-500 nm to make the channel shorter and to capture more photocarriers. In the present implementation, we estimated that 6-7 nanobeams were photoexcited. However a single nanobeam also supports a confined resonance[19] and therefore could be used for enhanced optical absorption in the channel.

Fabrication: The samples were fabricated from a molecular beam epitaxy grown heterostructure (wafer VA0757), consisting of a 270 nm think GaAs layer on top of a DBR stack. To achieve sub-picosecond carrier lifetime required for THz detectors, the top GaAs layer was grown at 250 °C. The DBR stack consisting of 5 pairs of $Al_{0.6}Ga_{0.4}As$/GaAs (60 nm/55 nm) was designed for high reflectivity at the excitation wavelength (800 nm). After the growth, the wafer was annealed at 600 °C for 40 s. The initial 270 nm thick GaAs layer was first etched to the thickness of ~160 nm using

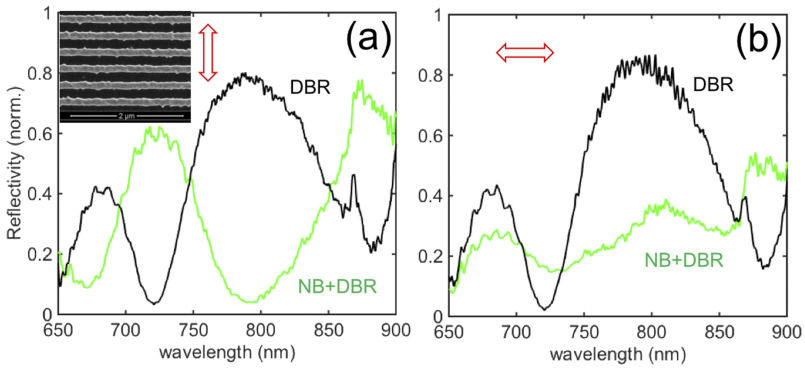

FIG. 4. Reflectivity spectra of the NB patch (green) for two orthogonal polarizations [(a) and (b)] indicated by the red arrows. The spectra are compared to the DBR reflectivity spectra (black). The inset shows an SEM image of the nanobeam patch.

Cl-based dry etching (*see below for details*) and then patterned with stripes arranged periodically (280 nm period) using electron beam lithography (EBL, *see below for details*). A range of different EBL exposures (180-250 μC/cm^2) was used to vary the width of the stripes. The surface was then dry-etched to the depth of ~70 nm to form the nanobeams with vertical walls. The structure was attached to a 0.5 mm thick sapphire substrate (unknown orientation) using epoxy (EPO-TEX 353ND) with the etched surface facing the sapphire substrate. The bulk GaAs wafer was removed by mechanical and chemical wet etching.[12] The remaining structure contained only the LT GaAs nanobeams on top of the 90 nm thick LT GaAs layer and the AlGaAs/GaAs DBR attached to the surface of the sapphire substrate. THz photoconductive antenna detectors were fabricated using EBL by depositing metallic contacts[11] with sharp points and a 1.5 μm gap, directly over the nanobeams.

Dry etching: An inductively coupled plasma system was used for dry etching. BCl_3, Ar, and N_2 were injected into the sample chamber at gas flow rates of 20, 2.5, and 4 standard cubic centimeter per minute, respectively. The radiofrequency sample chuck power was 240 W.

EBL: For electron beam lithography, we used PMMA950C resist (span at 3000 rpm for 30 s and baked at 180 °C for 180 s). Lithographic patterns were developed in a solution of IMBK:IPA (1:3) for 60 s and rinsed in IPA for 20 s.

See supplementary material for results of the experimental investigation of the THz detector response for different optical excitation powers and for reflectivity spectra of the metasurfaces fabricated with different nanobeam widths.

The authors acknowledge Michele Natrella for useful discussions. This work was supported by the Royal Society (Grant No. UF130493) and the EPSRC (Nos. EP/L015277/1 and EP/P021859/1), and it was performed, in part, at the Center for Integrated Nanotechnologies, an Office of Science User Facility operated for the U.S. Department of Energy (DOE) Office of Science. Sandia National Laboratories is a multi-mission laboratory managed and operated by National Technology and Engineering Solutions of Sandia, LLC., a wholly owned subsidiary of Honeywell International, Inc., for the U.S. Department of Energy's National Nuclear Security Administration under Contract No. DE-NA-0003525. I.B. acknowledges support of the U.S. Department of Energy, Office of Basic Energy Sciences, Division of Materials Sciences and Engineering.

[1] S. S. Dhillon *et al.*, J. Phys. D: Appl. Phys. **50**, 043001 (2017).
[2] D. H. Auston and M. C. Nuss, IEEE J. Quantum Electron. **24**, 184 (1988).
[3] M. Jarrahi, IEEE Trans. Terahertz Sci. Technol. **5**, 391 (2015).
[4] S. Lepeshov, A. Gorodetsky, A. Krasnok, E. Rafailov, and P. Belov, Laser Photonics Rev. **11**, 1600199 (2017).
[5] D. E. Aspnes, S. M. Kelso, R. A. Logan, and R. Bhat, J. Appl. Phys. **60**, 754–767 (1986).
[6] K. Peng, P. Parkinson, L. Fu, Q. Gao, N. Jiang, Y. Guo, F. Wang, H. J. Joyce, J. L. Boland, H. H. Tan, C. Jagadish, and M. B. Johnston, Nano Lett. **15**, 206 (2015).
[7] B. Heshmat, H. Pahlevaninezhad, Y. Pang, M. Masnadi-Shirazi, R. B. Lewis, T. Tiedje, R. Gordon, and T. E. Darcie, Nano Lett. **12**, 6255 (2012).
[8] C. W. Berry, N. Wang, M. R. Hashemi, M. Unlu, and M. Jarrahi, Nat. Commun. **4**, 1622 (2013).
[9] S. Jafarlou, M. Neshat, and S. Safavi-Naeini, Opt. Express **21**(9), 11115–11124 (2013).
[10] A. Jooshesh, L. Smith, M. Masnadi-Shirazi, V. Bahrami-Yekta, T. Tiedje, T. E. Darcie, and R. Gordon, Opt. Express **22**(23), 27992–28001 (2014).
[11] A. J. Macfaden, J. L. Reno, I. Brener, and O. Mitrofanov, Appl. Phys. Lett. **104**, 011110 (2014).
[12] O. Mitrofanov, I. Brener, T. S. Luk, and J. L. Reno, ACS Photonics **2**, 1763 (2015).
[13] M. Billet, P. Latzel, F. Pavanello, G. Ducournau, J.-F. Lampin, and E. Peytavit, APL Photonics **1**, 076102 (2016).
[14] R. J. Thompson, T. Siday, S. Glass, T. S. Luk, J. L. Reno, I. Brener, and O. Mitrofanov, Appl. Phys. Lett. **110**, 041105 (2017).
[15] S. Jahani and Z. Jacob, Nat. Nanotechnol. **11**(1), 23–36 (2016).
[16] Z. Yu, A. Raman, and S. Fan, Proc. Natl. Acad. Sci. U. S. A. **107**, 17491–17496 (2010).
[17] D. Liang *et al.*, Adv. Energy Mater. **2**, 1254–1260 (2012).
[18] A. P. Vasudev, J. A. Schuller, and M. L. Brongersma, Opt. Express **20**(S3), A385–A394 (2012).
[19] N. T. Fofang, T. S. Luk, M. Okandan, G. N. Nielson, and I. Brener, Opt. Express **21**, 4774 (2013).
[20] F. B. Arango, A. Kwadrin, and A. F. Koenderink, ACS Nano **6**(11), 10156–10167 (2012).
[21] I. Schwarz, M. G. Harats, N. Livneh, S. Yochelis, A. Strauss, A. Zimran, U. Banin, Y. Paltiel, and R. Rapaport, J. Opt. Soc. Am. B **29**(2), A127–A137 (2012).
[22] R. Magnusson and S. S. Wang, Appl. Phys. Lett. **61**, 1022–1024 (1992).
[23] Lumerical, Inc. http://www.lumerical.com/tcad-products/fdtd/.
[24] Normalization to the reflectivity spectrum of a gold patch positioned next to the detectors shows the reflectivity values in Fig. 4 as percentage of the light intensity reaching the semiconductor surface.